Polymer Degradation and Stability 228 (2024) 110930

Contents lists available at ScienceDirect

Polymer Degradation and Stability

journal homepage: www.journals.elsevier.com/polymer-degradation-and-stability

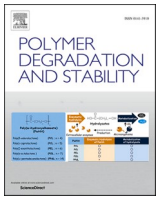

A study on the surface responses and degradation mechanisms of epoxy-amine coating subjected to UV accelerated weathering and hygrothermal ageing using ToF-SIMS and FTIR analysis

Janice Xin Yee Ng [a,*], Nicholas Sheng Loong Tan [a], Wing Huen Chung [b], Vladimir Golovanevskiy [a], Hanan Farhat [c], Thunyaluk Pojtanabuntoeng [a]

[a] Curtin Corrosion Centre, Curtin University, WA 6102, Australia
[b] School of Molecular and Life Sciences, Curtin University, WA 6102, Australia
[c] Corrosion Centre, Qatar Environment and Energy Research Institute, Hamad Bin Khalifa University, Qatar

ARTICLE INFO

Keywords:
Organic coatings
Thermal ageing
Accelerated weathering
UV
chemical properties
Epoxy
CUI
Corrosion under insulation
ToF-SIMS
FTIR
Principal component analysis

ABSTRACT

Epoxy amine coatings were subjected to hygrothermal ageing and accelerated weathering conditions that is comprised of neutral salt spray test and UV accelerated degradation condition. Time-of-flight secondary ion mass spectrometry (ToF-SIMS) and Fourier Transform Infrared Spectroscopy (FTIR) were employed to study the surface responses and spectral variation of epoxy amine coatings subjected to different ageing conditions. As a result, principal component analysis (PCA) of ToF-SIMS positive ion spectra illustrated that principal component 1 (PC1) has collected information on a variation of surface responses caused by accelerated weathering and hygrothermal ageing conditions as compared to fresh epoxy amine coatings. On the other hand, principal component 2 (PC2) has distinguished the different surface responses generated on epoxy amine coatings that were subjected to UV accelerated degradation conditions and those that were not. FTIR analysis has demonstrated the hydrolysis and photooxidation of epoxy amine coatings from the growth of two absorption bands at 1709 cm^{-1} and 1650 cm^{-1}, indicating the formation of carbonyl-containing groups such as ketones, aldehydes, phenyl formates, imine or tertiary amides. This comprehensive analysis provides significant insights into the degradation mechanisms of epoxy amine coatings subjected to corrosion under insulation (CUI) and/or artificial weathering (AW) environment. Understanding these mechanisms is pivotal for industries reliant on epoxy coatings, such as oil and gas, ensuring enhanced performance and extended lifespan of their products under varying environmental conditions. The findings also contribute to the broader field of materials science by offering methodologies and analytical approaches that can be applied to other polymeric coatings and materials.

1. Introduction

Epoxy coatings are extensively used in various industrial domains due to their wide range of attainable properties and versatilities [1]. For instance, epoxy coatings are generally utilised for corrosion under insulation (CUI) mitigation purposes as per NACE SP0198 [2]. However, degradation of epoxy coating surfaces under various conditions such as sunlight exposure, oxidation, moisture and high temperature may result in an alteration of the chemical and physical properties of the coating [1,3,4]. Therefore, different hardeners are added into epoxy resins to achieve different properties of the final coating products, such as to form highly crosslinked and chemically resistant coatings, to allow the room temperature curing of epoxy matrix, or to restrict the glass transition temperature of the epoxy coating at approximately 60 to 80 °C for optimum ductility and high thermal expansivity [4-6]. These desired attributes of epoxy coatings constrain the choices to a limited range of epoxide-amine combinations. Epoxy resins such as diglycidyl ether of bisphenol A (DGEBA) are commonly coupled with amine hardeners such as aliphatic amine hardener, isophorone diamine (IPDA), polyamidoamine (PAA) and triethylenetetramine (TETA) [4,7,8]. Nevertheless, a series of spectral changes arising from photooxidative or thermal oxidative ageing or hydrolysis such as the formation of phenyl formate groups [4,9-12], carbonyl groups [1,8,13-15], imine [7] or amides [11,13-15] has been reported when amine hardeners are incorporated. The

* Corresponding author.
E-mail address: janice.ng@curtin.edu.au (J.X.Y. Ng).

https://doi.org/10.1016/j.polymdegradstab.2024.110930
Received 3 March 2024; Received in revised form 17 July 2024; Accepted 22 July 2024
Available online 24 July 2024

degradation of epoxy coating surfaces and the formation of the aforementioned oxidative products would eventually act as a catalyst for exacerbated deterioration including physical alteration of epoxy coatings, ranging from thickness loss, mattifying effects, or variation of thermomechanical properties depending on the ageing conditions which would influence the residual stresses in the coating and ultimately result in crack initiation and propagation [15-20], amongst other potential failure modes.

The variation of chemical properties of epoxy coatings is commonly studied using Fourier Transform Infrared Spectroscopy (FTIR) [1,8,9,11, 13-16,18,21-24], time-of-flight secondary ion mass spectrometry (ToF-SIMS) [20,25-32], X-ray photoelectron spectroscopy (XPS) [20, 24], inductively coupled plasma mass spectrometry (ICP-MS), and liquid chromatography mass spectrometry (LC-MS) [27]. Despite significant attempts to fully characterise the chemical variation of epoxy amine coatings under a myriad of ageing conditions, there are still impediments to achieving a comprehensive characterisation. Therefore, ToF-SIMS, a highly sensitive surface analysis technique, was utilised in this research to illustrate the variation of the surface compositions of epoxy amine coatings subjected to UV irradiation and hygrothermal ageing respectively, whilst FTIR was utilised to disseminate information about the variation of chemical bondings, functional groups and molecular vibrations of the epoxy amine coatings under various ageing conditions. Nevertheless, the ionisation processes implemented in ToF-SIMS are intricate and thus, direct quantification of surface compositions variations are difficult. Therefore, multivariate calibration techniques such as principal component analysis (PCA) was utilised in this research to assist with the interpretation of data generated from ToF-SIMS.

Given the aforementioned influence of different ageing conditions on the thermomechanical properties, residual stresses development and chemical properties of organic coatings, this research focuses on the discussion of the influence of artificial ageing and/or hygrothermal ageing on the chemical properties of epoxy amine coating.

2. Experimental

2.1. Materials

A commercial epoxy amine coating (Humidur FP QR) was supplied and applied onto abrasive blasted 150 mm × 75 mm × 3 mm AS 1594 HA 250 carbon steel panels with an average surface profile of 50 to 75 μm to obtain average dry film thickness (DFT) of 607 ± 55 μm at room temperature (23 ± 2 °C) as per the coating manufacturer's recommendation. The coated panels were subsequently cured at 23 ± 2 °C and 50 ± 5 % relative humidity for 24 h prior to being subjected to accelerated weathering and/or simulated CUI ageing tests (hygrothermal ageing), described below.

Fresh, and aged, coated specimens were cut into 20 mm × 20 mm × 3 mm specimens using a waterjet cutting machine (MICRACUT 202 Precision Cutters) and degreased with 99 % ethanol prior to ToF-SIMS analysis. Coated specimens was left to cure at 23 ± 2 °C and 50 ± 5 % relative humidity for 24 h prior to the acquisition of dry and fine coating power specimens using Dremel 32 mm 426 fibreglass reinforced cut-off wheels for FTIR analysis.

2.2. Artificial weathering

8 weeks of artificial weathering was adapted from the cyclic ageing test described in ISO 12944–6:2018 [33]. Each cycle of the artificial weathering comprised of three days of UV/condensation, four days of neutral salt spray test and one day of low temperature exposure at −20 °C.

UV/condensation tests were conducted using a PAC-540-A-3K Climatic Chamber (CM Envirosystems) and the estimated irradiance of the UV test is approximately 16.60 W/m^2. Coated panels were mounted vertically on the specimen holders in the climatic chamber fitted with a UV-A lamp (OSRAM Ultra Vitalux UV-A E27). UV/Condensation cycle mode was then initiated and with the operating temperature set to run from room temperature to 45 ± 2 °C. The specimens were removed from the climatic chamber after the three-day UV/condensation test and moved to the neutral salt spray test chamber immediately after the test.

Neutral salt spray test was conducted using the SF-450-CCT Cyclic Corrosion Test Chamber (C&W Specialist Equipment Limited CCT) from room temperature (23 ± 2 °C) to 65 °C and relative humidity of 25 ± 5 % to 95 ± 5 %. Coated panels were fitted horizontally into specimen holders in the neutral salt spray test chamber and the solution tank at the back of the chamber was topped up with 5 wt.% sodium chloride (NaCl) solution. Coated specimens were rinsed with deionised (DI) water after the completion of the 4-day-neutral salt spray test prior to switching to the low temperature exposure in the climatic chamber.

Coated panels were mounted vertically on the specimen holders in the climatic chamber and the low temperature cycle was initiated. The low temperature cycle was conducted at −20 °C and UV/condensation cycle was initiated again for the subsequent tests upon the completion of the low temperature cycle.

2.3. Hygrothermal ageing

Hygrothermal ageing test setup was designed based on the setup in Yang, et al. [34] to simulate a corrosion under insulation (CUI) environment. The ageing cycles were adapted from the vertical pipe test described in ISO 19277:2018 [35]. 200 mm × 300 mm × 50 mm thermal insulation (Rockwool) slabs were saturated in 1 wt.% sodium chloride solution for 30 days prior to hygrothermal ageing. A drainage hole was drilled at the bottom of the baking tray for the draining of NaCl solution after each NaCl solution refill. All coated panels were placed in 200 × 300 mm carbon steel trays on a 600 mm × 400 mm digital hot plate (LA-SSH-E600D) and the saturated thermal insulation slabs were placed on top of the panels.

The trays were then covered with an aluminium lid. The coated panels were heated in this system at 150 °C for 8 h per day for 5 days per week over an 8-week period. The system was turned off after the 8-hour heating every day and allowed to cool to room temperature (23 ± 2 °C), followed by the addition of 3 L of 1 wt.% NaCl solution from the drilled holes on the aluminium lid. Excess NaCl solution was drained from the systems and the systems were kept at room temperature, prior to the next heating cycle in the morning. Coated panels were rinsed with DI water after 8 weeks of hygrothermal ageing and subjected to FTIR and ToF-SIMS testing.

2.4. Time of flight simulation (ToF-SIMS)

ToF-SIMS analyses were performed using a IONTOF ToF-SIMS M6 instrument (IONTOF GmbH, Germany) equipped with a reflectron mass analyser, a 30 keV Bi cluster nanoprobe, and a 20 keV gas cluster ion beam (GCIB) for sputtering and analysis. Positive ion high mass resolution spectra (> 7500 at $m/z = 29$) were acquired from five 100 μm × 100 μm areas from each specimen using a cycle time of 100 μs. All the peaks within the range of 0 to 300 m/z were selected and the mass spectra obtained in ToF-SIMS were calibrated and smoothed. The ion intensities acquired were then used for principal component analysis (PCA).

2.5. Principal component analysis (PCA)

PCA is a multivariate analysis (MVA) technique that is generally utilised to enhance the interpretation of the substantial number of datasets, such as those generated by ToF- SIMS. Principal component analysis (PCA) in this work was conducted using OriginLab 2022 software (Origin Lab Corporation, Massachusetts).

2.6. Fourier transform infrared spectroscopy (FTIR)

FTIR spectra for coating specimens were obtained using a Nicolet iS50 FTIR spectrometer equipped with a single-bounce diamond crystal (iS50-ATR attachment). FTIR measurements were undertaken in transmittance mode over wavelength ranging from 4000 to 400 cm^{-1}, with resolution of 4 cm^{-1} and addition of 64 scans. Collection of data was performed using the OMNIC software (version 9.1.2.4) with background spectrum obtained prior to every measurement. Data normalisation and visualisation were conducted using OriginLab 2022 software (Origin Lab Corporation, Massachusetts). The FTIR spectra was normalised using aromatics peak at around 3100–3000 cm^{-1}.

3. Results and discussion

3.1. Time of flight simulation (ToF-SIMS) and principal component analysis (PCA)

Discoloration and a matte and dull layer was observed on the epoxy amine coating after artificial weathering, and a similar observation was reported in Rezig, et al. [15], Brand, et al. [27], where this observation was suggested to be attributed to the breakage of epoxy polymeric matrix, which led to a further degradation of the resin. Therefore, ToF-SIMS analysis were undertaken in this research to investigate the surface molecular differences between surfaces of epoxy amine coating specimens that were subjected to different ageing conditions. The average ion intensities of epoxy amine coatings subjected to different ageing conditions versus mass-to charge ratio (m/z) is shown in Figs. 1 and 2.

PCA of positive secondary ions shown in Figs. 1 and 2 acquired through TOF-SIMS of 100μm × 100μm areas has resulted in the identification of two principal components (PC1 and PC2) as shown in the biplot in Fig. 3.

Based on Fig. 3, PC1 and PC2 has captured 51.83 % and 31.48 % of the total variance. According to the Kaiser-Guttman's PCA rule, two components (PC1 and PC2) were included in the discussion of this study to explain the existing dataset, and the cumulative score of 83.31 % indicated a good level of representation. The mass fragments corresponding to the assigned labels in Fig. 3 are tabulated in Table 1.

PCA has provided notable differences between epoxy amine coatings subjected to different ageing conditions. Information gathered by PC1 has segregated AW, AWCUI, CUI and fresh specimens into two groups based on Fig. 3. The first group is comprised of epoxy amine coating specimens that were subjected to artificial weathering (AW), hygrothermal ageing (CUI) and artificial weathering followed by hygrothermal ageing (AWCUI); the second group is constituted of epoxy amine coating specimen that was not subjected to any ageing condition (fresh). Based on Fig. 3, AW, AWCUI and CUI specimens shared a higher similarity of surface molecular mass fragments but are negatively correlated with fresh specimens. This variance could be an indication of deterioration or variation of surface compositions of epoxy amine coatings as a result of various chemical reactions, especially those that has resulted in an increase in element "R" as shown in Fig. 3, that represents mass fragment Mg^+, and those that has resulted in a reduction in aliphatic hydrocarbon ions illustrated in PC1 axis. Next, PC2 has categorised the epoxy amine specimens into two groups based on the 31.84% of variance between these specimens, with AWCUI and AW specimens being grouped into the same category and CUI and fresh specimens in the other. This indicates a higher similarity of surface compositions was shared between AWCUI and AW specimens whilst a dissimilarity was observed in CUI and fresh specimens. Thus, it is suggested that PC2 has illustrated a variation of surface compositions caused by artificial weathering.

According to PC1 as presented in Fig. 3, component R which is a representation of Mg^+ mass fragment has a positive correlation to AW, AWCUI and CUI specimens whilst $C_5H_2^+$, $C_5H_3^+$, $C_6H_2^+$, $C_6H_4^+$, $C_7H_3^+$, $C_7H_5^+$, $C_8H_6^+$, $C_8H_7^+$, $C_9H_{10}^+$, $C_{10}H_7^+$, $C_{11}H_7^+$ $C_{12}H_8^+$, $C_{13}H_9^+$, $C_{14}H_8^+$, $C_2H_2^+$, $C_{14}H_{13}O_2^+$ has a negative correlation to AW, AWCUI, and CUI specimens. The increase in Mg^+ mass fragments that has an m/z value of 23.98 amongst aged specimens have been observed in Fig. 1, with the highest ion intensity generated on AWCUI specimen's surface, followed by CUI, Fresh and AW specimens. Mg^+ mass fragments could be originating from magnesium hydroxide, magnesium oxide or magnesium silicate particles that are generally utilised as functional fillers in epoxy resins as flame retardants or to enhance mechanical properties of the coating [36.40]. Based on the ion intensities of Mg^+ mass fragments on the epoxy amine coating surfaces, AWCUI treatment may have had the largest impact on the degree of degradation of epoxy amine coating as compared to other ageing conditions and the increase in Mg^+ions could be attributed to the significant deterioration of the polymer matrix, thereby, exposing the underlying surface containing these magnesium-based fillers [41].

Next, aliphatic hydrocarbon ions such as $C_5H_2^+$, $C_5H_3^+$, $C_6H_2^+$, $C_6H_4^+$, $C_7H_3^+$, $C_7H_5^+$, $C_8H_6^+$, $C_8H_7^+$, $C_9H_{10}^+$, $C_{10}H_7^+$, $C_{11}H_7^+$ $C_{12}H_8^+$, $C_{13}H_9^+$, $C_{14}H_8^+$, $C_2H_2^+$, $C_{14}H_{13}O_2^+$ that are negatively correlated to AW, AWCUI and CUI specimens are mainly constituted of alkenyl (C_nH_{2n-1}), alkenes or alkyls (C_nH_{2n+1}), unsubstituted monocyclic hydrocarbon (C_nH_n), and alkanes (C_nH_{2n+2}). Based on Figs. 1 and 2, there is a general trend of reduction of ion intensities of the aforementioned aliphatic hydrocarbon ions after the specimens were being subjected to different ageing conditions, with the highest ion intensities measured on the surfaces of fresh specimens and the lowest ion intensities measured on the surfaces of the AWCUI specimens. These hydrocarbon ions could be attributed to the hydrolytic degradation of epoxy amine coatings and the reduction of these ions could be an indication of the reduction of polymeric network density as a result of hydrolysis that could be acquired during hygrothermal ageing or primary epoxy chain scission reactions as a result of UV irradiation [7,9,10,21,42,43]. Hydrolytic degradation of epoxy amine coatings is mainly constituted diffusion [5,44,45], absorption [5,44,45], hydrolysis [44], plasticisation [44], and/or chain scission [44]. Diffusion of water into the polymeric network is initiated during the accumulation of water on the accessible nanopores of the epoxy amine surfaces during the exposure to NaCl solution.

In cases where there is a raise of temperature during the hygrothermal ageing process or given a high polarity of the epoxy amine coating, additional void nanopores that are localised at the crosslink junctions in the polymeric structure are created as a result of thermal expansions and molecular vibrations [3,44,45]. The aforementioned crosslink junctions are also the location of polar hydroxyls and amines and the void nanopores would allow the polymeric matrix to be opened and the polar sites to be revealed, which would ultimately result in the enhanced facilitation of the access of water to the interaction sites [3,44,45]. This would lead to a reaction between water molecules and the ether groups that are created during the polymerisation reaction between epoxy and amine [22]. Subsequently, hydrophilic groups would be generated, and this would lead to the increase of water absorption rate of the polymer. The water absorption process of epoxy amine coating obeys the Fick's law of diffusion, and the rate of absorption is mainly dependent on the chemical formulation of the coating [19,22]. Consequently, hydrolysis is eventuated, where the hydrogen bonds between polymeric segments are dismantled due to the absorption of water and this would exacerbate the production of hydrophilic groups followed by the reduction of crosslink density of the polymer [22,44]. During hydrolysis, the chain mobility of the polymer is increased, and low molecular weight species are able to manoeuvre away from the original polymeric network. This would then lead to plasticisation or more severe deterioration to the epoxy such as chain scission [3,16,17,19,22,44]. As a result, unstable structural fragments, such as the aforementioned low molecular weight hydrocarbon ions and oxygen-containing species may be liberated from the epoxy-amine surfaces during ToF-SIMS operation [20]. $C_{14}H_{13}O_2^+$ is suggested to be attributed to bisphenol A resulting from the loss of a methyl group based

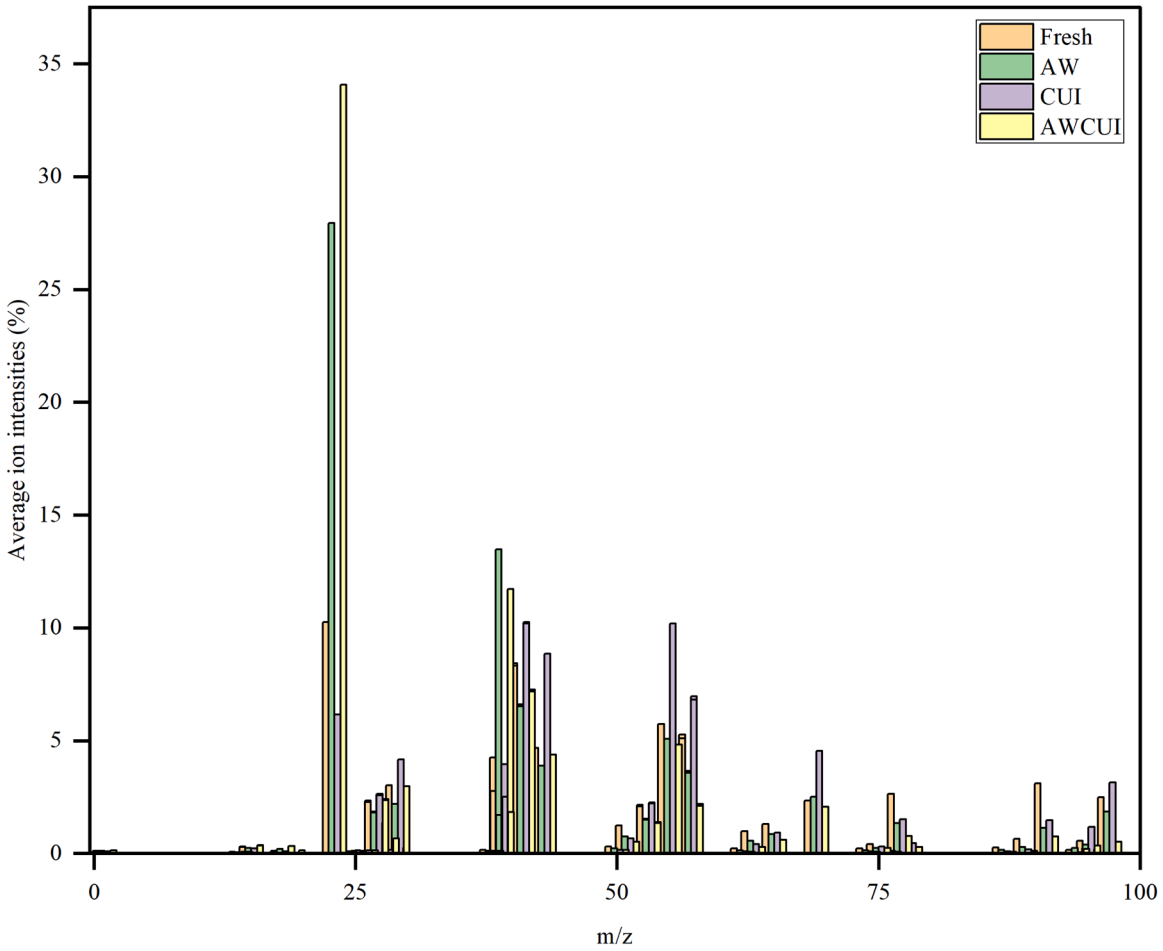

Fig. 1. Average ion intensities versus *m/z* of epoxy amine coatings subjected to different ageing condition (0 to 100 *m/z*).[11].

on Sambaza, et al. [46]. The reduction of these fragments would further suggest a degradation of the epoxy-amine polymer as per the aforementioned hydrolytic degradation mechanism. Reaction of epoxy amine coatings towards various thermal conditions are generally reflected by the intrinsic reactivity of hydrocarbon ions when being subjected to mild or high temperature conditions [47]. The aforementioned aliphatic hydrocarbon ions could also be effectuated from primary epoxy chain scission reaction at multiple points in the epoxy structure after being subjected to UV irradiation, and were thus, liberated as volatile fragments during ToF-SIMS operation [20].

The hydrocarbon ions could also be originating from aliphatic polyethers from polyether amine that is generally utilised in the formulation of anticorrosive epoxy-amine coatings, that were fragmented into smaller-sized hydrocarbon ions during ToF-SIMS operations [48]. Aliphatic polyethers exhibit notable susceptibility to photooxidation when being subjected to UV. The photooxidation reaction of polyethers is generally initiated with the subtraction of hydrogen atom from the alpha-carbon (α-carbon) atom in the ether structure [9]. Awaja, et al. [32,48] has associated the increase of aliphatic hydrocarbon ions to: (1) the formation of a denser network through branching and crosslinking reactions and (2) the totality of the degree of cure of epoxy resins; and have established a direct correlation of the aforementioned phenomena to the curing reaction time. Therefore, the inverse correlation between aliphatic hydrocarbon ions and aged epoxy amine coatings that was observed in this work was suggested to be an indication of degradation of the epoxy amine coatings after being subjected to different ageing conditions.

Subsequently, based on PC2 as illustrated in Fig. 3, CH_3^+ (methyl cations) that is represented by label M and N has a positive correlation with AWCUI and AW whilst $C_3H_5^+$ and $C_8H_5O^+$ that is represented by label AF, AG and BK has a negative correlation with the aforementioned epoxy amine specimens. Based on Fig. 1, the highest ion intensity of CH_3^+ is found on AWCUI specimen's surface and these methyl cations could be attributed to methyl or alkyl constituents in the epoxy amine coating [47]. Epoxy amine coating may have undergone a higher degree of degradation as a result of the combined effects of photo- and thermo-oxidative degradation arising from AWCUI ageing, which may have led to the formation of radical species, followed by subsequent formation of smaller hydrocarbon species that consist of CH_3^+groups [7,8]. Next, based on Fig. 1, the highest ion intensities of hydrocarbon ions such as $C_3H_5^+$ and $C_8H_5O^+$ were measured on CUI specimen's surface, and the generation of these hydrocarbon ions are suggested to follow the same mechanisms as those observed in PC1.

3.2. Fourier transform infrared spectroscopy (FTIR)

FTIR analysis as a function of different ageing conditions has shown a significant spectral variation after hygrothermal ageing of epoxy-amine coating as illustrated in Fig. 4 and the vibrational modes of these absorption bands are tabulated in Table 2.

Attempts were undertaken to identify the absorption bands from the region of 4000 cm^{-1} to 450 cm^{-1} as tabulated in Table 2. In the fresh specimen, the characteristic signals of the hydroxyl group were presented as an intense broad band around 3364 cm^{-1}, representing the stretching vibration of the O—H bond and is also present in all four specimens. Absorption peak around 3100 – 3000 cm^{-1} is associated with sp^2 C—H stretching vibrational mode originating from aromatic chemical structures. The band centred around 2920 cm^{-1} is associated with

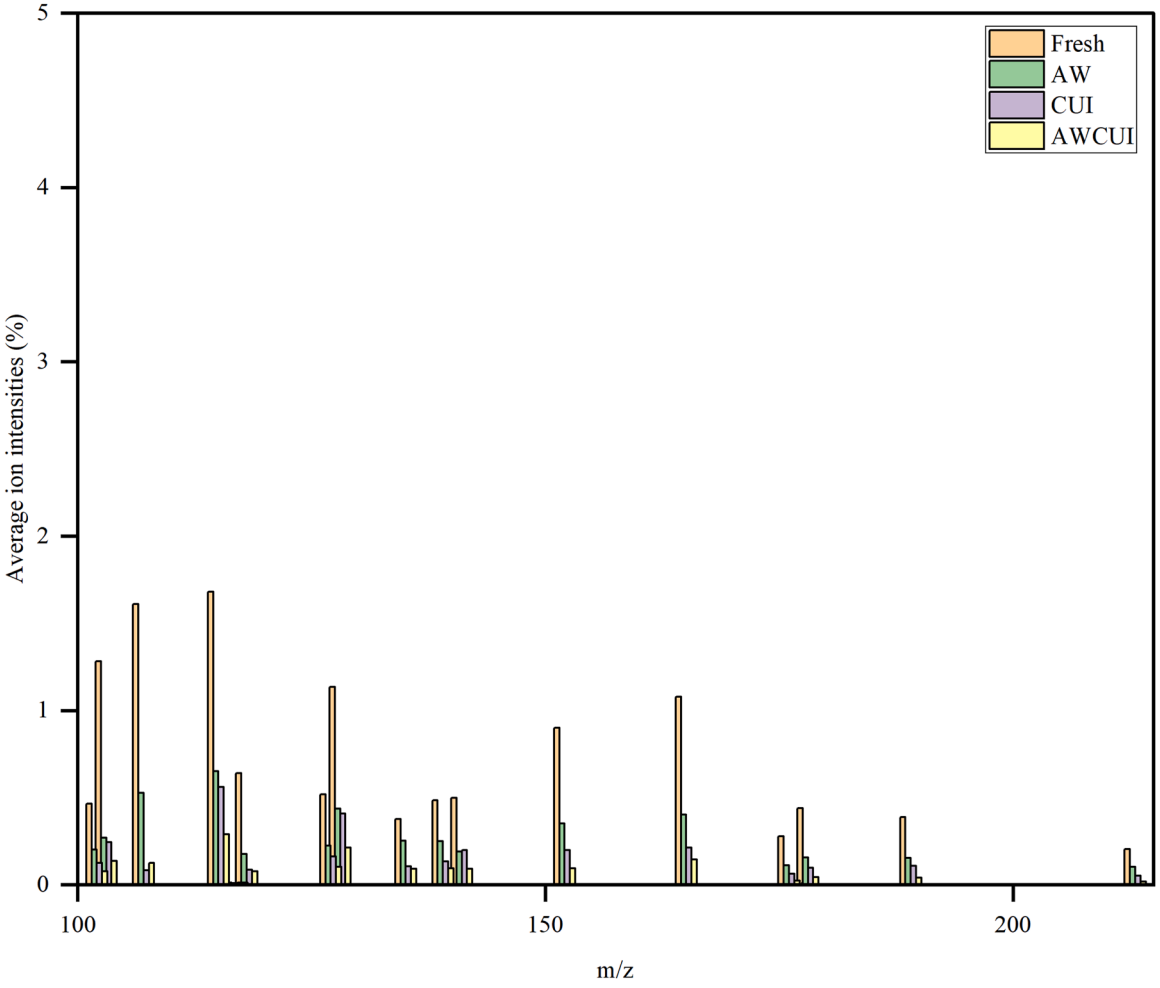

Fig. 2. Average ion intensities versus *m/z* of epoxy amine coatings subjected to different ageing condition (100 to 220 *m/z*).[21].

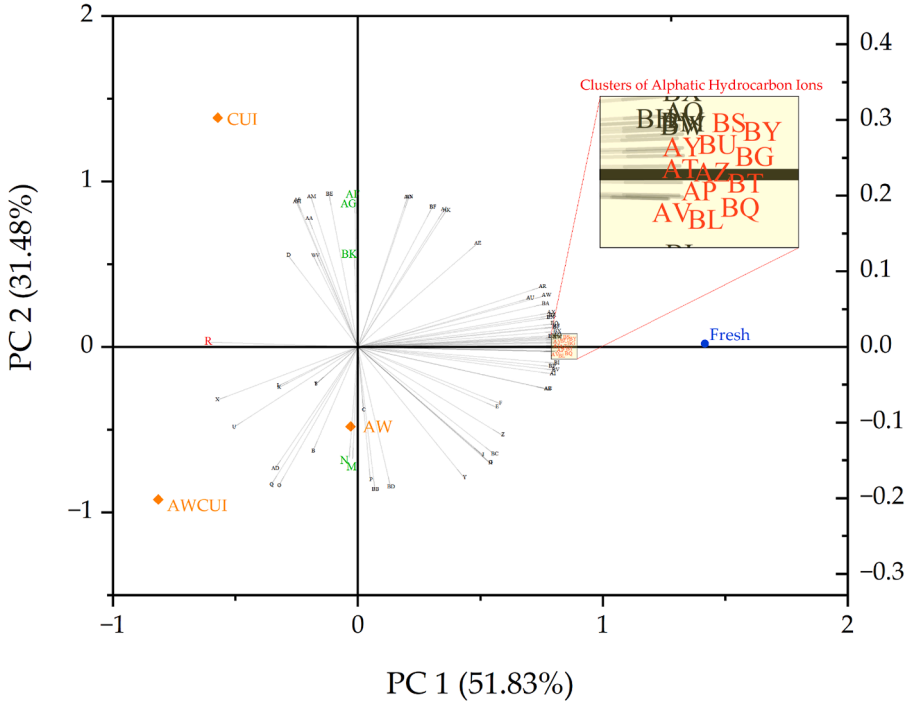

Fig. 3. Principal component analysis biplot of positive secondary ions illustrated in Fig. 1 and 2.

Table 1
Correspondence of mass fragments to assigned labels in Fig. 3 and extracted eigenvectors.

Label	Mass fragment	PC1	PC2	Label	Mass fragment	PC1	PC2	Label	Mass fragment	PC1	PC2	Label	Mass fragment	PC1	PC2
B	H^+	−0.04	−0.14	U	Al^+	−0.10	−0.11	AN	$C_4H_9^+$	0.04	0.20	BG	$C_8H_6^+$	0.16	0.00
C	H_2^+	0.00	−0.08	V	$C_2H_3^+$	−0.03	0.12	AO	$C_4H_5^+$	0.04	0.20	BH	$C_8H_7^+$	0.15	0.01
D	H_3^+	−0.06	0.12	W	$C_2H_3^+$	−0.04	0.12	AP	$C_5H_2^+$	0.16	−0.01	BI	$C_7H_7O^+$	0.16	−0.02
E	$^6Li^+$	0.11	−0.08	X	Si^+	−0.11	−0.07	AQ	$C_5H_3^+$	0.16	0.02	BJ	$C_9H_7^+$	0.16	0.03
F	Li^+	0.11	−0.07	Y	CH_2N^+	0.08	−0.17	AR	$C_5H_5^+$	0.15	0.08	BK	$C_8H5_O^+$	0.00	0.12
G	C^+	0.11	−0.15	Z	CHO^+	0.12	−0.12	AS	$C_5H_9^+$	−0.05	0.19	BL	$C_9H_{10}^+$	0.16	−0.01
H	C^+	0.11	−0.15	AA	$C_2H_5^+$	−0.04	0.17	AT	$C_6H_2^+$	0.16	0.00	BM	$C_{10}H_7^+$	0.16	0.01
I	CH^+	0.10	−0.14	AB	$C_3H_2^+$	0.15	−0.06	AU	$C_6H_3^+$	0.14	0.06	BN	$C_9H_4O^+$	0.15	0.04
J	CH^+	0.10	−0.14	AC	$C_3H_2^+$	0.15	−0.06	AV	$C_6H_4^+$	0.16	−0.01	BO	$C_{10}H_8^+$	0.16	0.03
K	CH_2^+	−0.06	−0.05	AD	K^+	−0.07	−0.16	AW	$C_6H_5^+$	0.15	0.07	BP	$C_9H_{11}O^+$	0.15	−0.03
L	CH_2^+	−0.06	−0.05	AE	$C_3H_3^+$	0.10	0.14	AX	$C_6H_6^+$	0.15	0.05	BQ	$C_{11}H_7^+$	0.16	−0.01
M	CH_3^+	0.00	−0.15	AF	$C_3H_5^+$	0.00	0.19	AY	$C_7H_3^+$	0.16	0.01	BR	$C_{11}H_9^+$	0.15	0.04
N	CH_3^+	−0.01	−0.15	AG	$C_3H_5^+$	0.00	0.19	AZ	$C_7H_5^+$	0.16	0.00	BS	$C_{12}H_8^+$	0.16	0.01
O	NH_4^+	−0.06	−0.18	AH	$C_3H_7^+$	−0.05	0.19	BA	$C_7H_7^+$	0.15	0.06	BT	$C_{13}H_9^+$	0.16	0.00
P	H_3O^+	0.01	−0.18	AI	$C_4H_2^+$	0.16	−0.04	BB	$C_6H_6O^+$	0.01	−0.19	BU	$C_{14}H_8^+$	0.16	0.01
Q	Na^+	−0.07	−0.18	AJ	$C_4H_3^+$	0.16	0.03	BC	$C_6H_7O^+$	0.11	−0.14	BV	$C_{13}H_6O^+$	0.16	−0.03
R	Mg^+	−0.12	0.01	AK	$C_4H_5^+$	0.07	0.18	BD	$C_6H_7O^+$	0.03	−0.19	BW	$C_2H_2^+$	0.16	0.01
S	$C_2H_2^+$	−0.03	−0.05	AL	$C_4H_5^+$	0.07	0.18	BE	$C_7H_{11}^+$	−0.02	0.20	BX	$C_{15}H_9^+$	0.16	0.02
T	$C_2H_2^+$	−0.03	−0.05	AM	$C_4H_7^+$	−0.04	0.20	BF	$C_7H_{13}^+$	0.06	0.18	BY	$C_{14}H_{13}O_2^+$	0.16	0.01

the sp^3 C—H symmetric and antisymmetric stretching attributed to the alkyls in the material. The absorption bands appearing at around 1600 – 1450 cm^{-1} are vibrational modes from the C—C ring stretching which could be combination of mixtures of para- and ortho-disubstituted aromatic chemical species which can be attributed to the presence of regioisomers as result of oligomeric reaction product between bisphenol A and epichlorohydrin which is typical in commercial epoxy resins [51]. The bands associated with secondary alcohol as result of the ring opening reaction of the oxirane ring are the O—H deformation mode at 1296 cm^{-1} and C—O stretching modes at 1105 cm^{-1}. The absence of the C—O—C bending mode of oxirane ring at 915 cm^{-1} suggests a complete ring opening reaction [52]. Other notable bands identified are associated with P-O symmetric stretching and bending modes at 947 cm^{-1} and 633 cm^{-1} which originates from zinc phosphate which is added as a corrosion inhibitor additive based on Hao, et al. [53], which is present in the current material based on its material safety data sheet.

Spectral subtraction was performed between fresh (reference spectrum) and aged specimens to facilitate the study the loss or gain in bands in the IR spectrum as shown in Fig. 5. The following absorption band were observed to decrease after applying the ageing treatments and these are the secondary alcohol (O—H deformation and C—O stretching modes), C—C aromatic ring stretching modes, and phenyl ether C—O—C symmetric and antisymmetric stretching modes. Decrease in aromatic ring signals could be due to loss of solvent molecules such benzyl alcohol which is the non-reactive diluent use in this formulation. There was an observable increase in the absorption band at 1709 cm^{-1} which is associated with the formation C = O from ketones and at 1650 cm^{-1} C=*O* which could be attributed to the formation of tertiary amide or imine due to oxidation processes with greatest intensity achieved after applying the harshest ageing treatment which is a combination of hygrothermal (CUI) and UV ageing (AWCUI). Consumption of the phenyl ether C—O—C bands at 1239 cm^{-1} (antisymmetric stretch) and 1028 cm^{-1} (symmetric stretch) after ageing treatments are consistent with photo-Fries rearrangement process which is well regarded photo-oxidation degradation mechanism reported in literature Rivaton [54].

An increase in the intensity with the band associated with sp^3 C—H symmetric and antisymmetric stretching was observed with hydrothermal (CUI) and combination (AWCUI) ageing treatment accompanied by an increase with O—H band as well.

N—H peaks from residual unreacted amines were identified and subsequent peak area ratio analysis was attempted to determine the extent of curing under different ageing treatments. However, the typical vibrational mode(s) of primary and secondary amines above 3000 cm^{-1} that is associated with N—H stretching were not easily identifiable in the FTIR spectrum. Conversely, a vibrational mode at 699 cm^{-1} in the fingerprint region was identified and it may be ascribed to N—H wagging (either primary or secondary). A reduction of intensity was observed from specimens subjected to CUI ageing conditions, with a percentage decrease of 34% in peak area compared to AW ageing that demonstrated a 3% decrease in peak area. This observation is consistent with the fact that further curing is facilitated by high heat (under CUI conditions). This is also apparent in the AWCUI ageing regime, where a 26% decrease in the peak area was also noted where heating was also present.

The increase of O—H group at 3364 cm^{-1} as illustrated in Fig. 5 was observed after epoxy amine coating was subjected to UV irradiation and hygrothermal ageing respectively and this phenomenon is suggested to be attributed to the oxidation of aromatic alcohols [24,55]. This could also be seen from the generation of higher fragmentation on aged specimens during ToF-SIMS, especially on AWCUI specimen surfaces as shown in Figs. 1 and 2. Epoxy coatings in general, consist of aromatic groups that have a strong UV absorption range of approximately 300 nm. This culminates in a vulnerability in the epoxy structures when the coating is being subjected to UVA and UVB irradiation. The average photon energy of UVA and UVB is 399 kJ/mol and 428 kJ/mol respectively whilst the bond energy of C—O and C—C bond is around 316 kJ/mol and 347 kJ/mol respectively [56]. Therefore, C—C and C—O bonds in the epoxy-amine material are prone to breaking when subjected to UV irradiation which can result complex UV degradation mechanisms depending on the chemical moieties undergoing photooxidation reactions [11,57].

Subsequently, a strong and sharp band at around 2920 cm^{-1} attributed to alkyl or alkane functional groups, representing the C—H stretching vibration is observed in all four specimens. C—H stretching vibration is associated with a wide range of organic compounds and it is relatively common for organic compounds such as propylene, to contain long chains of single-bonded carbon atoms such as alkane and thus, spectra of these organic compounds would be dominated by alkane signatures [58]. It is proposed that the sp^3 hybridised C—H stretching in

[1] ToF SIMS data was collected from five locations per specimen, with each m/z count normalised by the total counts at each spot and expressed as a percentage. These percentages were then averaged across the five locations for each specimen.

[2] ToF SIMS data was collected from five locations per specimen, with each m/z count normalised by the total counts at each spot and expressed as a percentage. These percentages were then averaged across the five locations for each specimen.

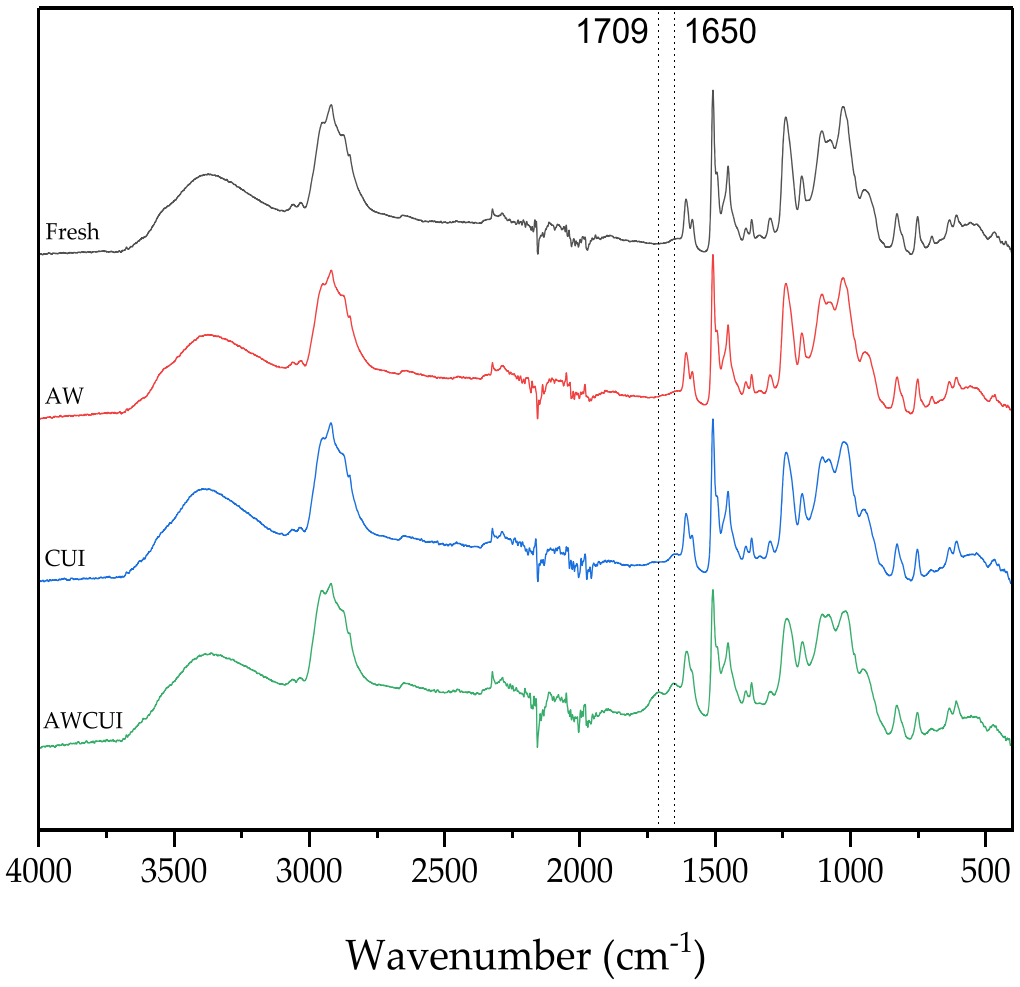

Fig. 4. FTIR spectra of epoxy amine coated specimens under different ageing conditions.

Fig. 4 is mainly dominated by the methyl group present in the diglycidyl ether bisphenol A (DGEBA) resin backbone, which is a common building block for highly cross-linked epoxy resin networks. As seen in Fig. 4, significant increase of the intensity of C—H stretching vibration is evident in specimens subjected to artificial weathering and/or hygrothermal ageing, which could be attributed to the photooxidative degradation of the aforementioned methyl group, and this observation is supported by the ToF-SIMS outcome presented in Figs. 1 and 2, where

Table 2
Relevant absorption bands, the associated vibrational mode and functional groups where identifiable from IR spectrum of fresh and aged specimens.

Absorption band (cm^{-1})	Vibrational mode	Functional groups
3364	O-H stretching	Alcohol
3100 - 3000	sp^2 C—H stretching	Aromatics
2920	sp^3 C-H stretching	Alkyl/alkane
1709	C = O stretching	Ketones
1650	C = O stretching or C = N stretching	Tertiary amide or imine
1608	C-C ring stretching	Mixture of para- or ortho-disubstituted aromatic ring
1584	C-C ring stretching	Mixture of para- or ortho-disubstituted aromatic ring
1508	C-C ring stretching	Mixture of para- or ortho-disubstituted aromatic ring
1452	C-C ring stretching	Mixture of para- or ortho-disubstituted aromatic ring
1386	n/a	n/a
1365	n/a	n/a
1334	C-H deformation	Alkane
1296	O—H deformation	Secondary alcohol
1239	C—O—C antisymmetric stretching	Phenyl ether
1180	C—H in-plane H bend	p-disubstituted aromatic ring
1105	C-O stretching	Secondary alcohol
1026	C—O—C symmetric stretching	Phenyl ether
947	P-O symmetric stretching	Phosphate, PO_4^{3-} [49,50]
828	Two Adjacent C—H out-of-plane (oop) deformation	para-disubstituted aromatic ring
752	C-H oop deformation	ortho-disubstituted aromatic ring
699	N-H wagging	Primary or secondary amine
633	P—O bending	Phosphate, PO_4^{3-} [49,50]
608	n/a	n/a
556	n/a	n/a
468	n/a	n/a

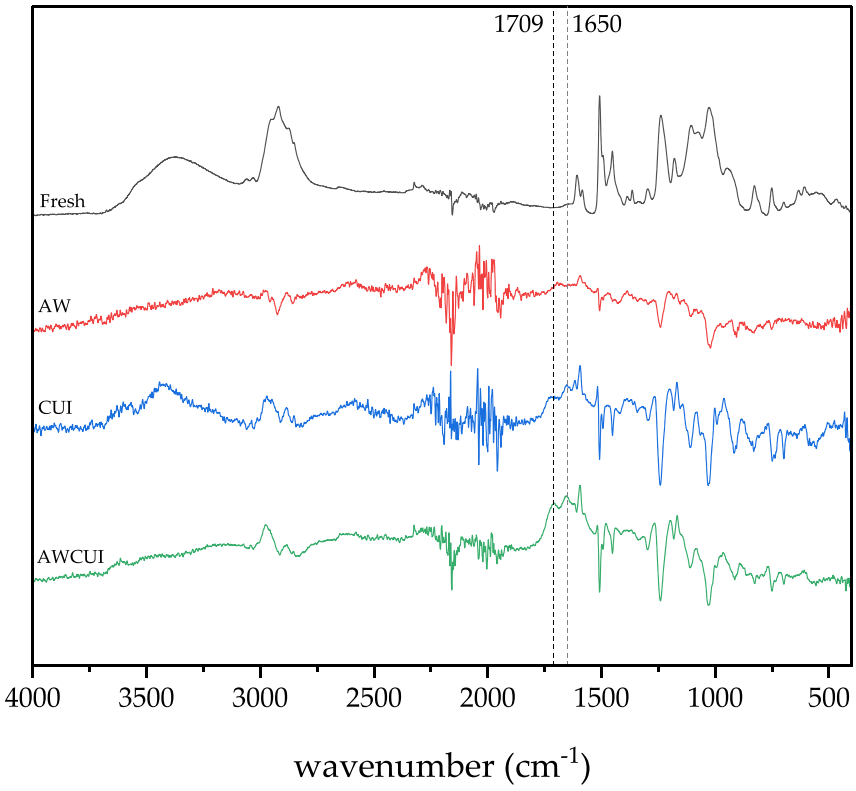

Fig. 5. Appearance of a new absorption band in the FTIR of the aged specimens after subtracting the fresh specimen (reference spectrum); carbonyl peaks (vertical dash line) at 1709 cm^{-1} and 1650 cm^{-1} associated with ketone and tertiary amide or imine functionality respectively.

higher amount of fragmentations were generated on aged specimens' surfaces as compared to fresh specimens' surfaces. The degradation mechanism of methyl group as a photo-initiating site that ultimately resulted in the formation of carbonyl groups has been discussed in Ghasemi-Kahrizsangi, et al. [1], where, methyl radical and hydroxyl radical are formed from the photodissociation of methyl hydroperoxide, followed by the formation of carbnyl group following the addition of molecular oxygen.

The presence of the carbonyl functional group that is generally associated with the oxidative degradation of diglycidyl ether bisphenol A (DGEBA) moiety of the epoxy amine coating [7-9,21] is apparent from the stretching frequency of the C=O bond at 1709 cm^{-1} and 1650 cm^{-1}, and these bands were observed in specimens subjected to AWCUI and CUI ageing conditions. Based on Fig. 4, high temperature exposure during CUI conditions proceeding the artificial weathering conditions have resulted in the most significant changes in the specimens. The formation of carbonyl containing functional groups within the range of 1600 to 1800 cm^{-1} is also presented in Fig. 4, in which the result aligned with findings obtained from other analyses in this study.

The appearance of absorbance at 1709 cm^{-1} as shown in Fig. 5, could be attributed to aldehyde or ketone stretching vibration, or phenyl formates. While the absorbance at 1650 cm^{-1} could be accounted as tertiary or secondary amides [7,13]. The lack of characteristic amide II band in the usual region (attributed to the combination band of C—N and N—H bending) suggest it is predominantly tertiary amide [59]. Photooxidative degradation of polymers such as epoxy coatings is generally constituted of several reactions, such as chain scission, excessive cross linking between polymeric segments and/or the formation of radical species as a result of photo-induced oxidation reaction [60,61]. These radicals can be further oxidised to form hydroperoxides followed by carbonyl containing groups. Formation of carbonyls are mainly due to the degradation of methyl group in the epoxy chain due to the low bonding energy of methyl groups to the main epoxy chain [1, 10]. This theory can be further validated from the reduction of O—H stretching vibration at 3364 cm^{-1} after the epoxy amine coatings were subjected to UV irradiation. Carbonyls have the tendency to absorb light at certain wavelengths, followed by the transmittal and reflection of other wavelengths. This generally leads to discolouration in epoxy coatings when UV irradiation is involved [1,8]. The formation of phenyl formate at 1709 cm^{-1} is proposed to follow the mechanisms reported in Rivaton, et al. [10], Nikafshar, et al. [11] and Malajati, et al. [12]. During the photooxidation of phenoxy resins, oxidation of methylene (CH_2) group that is located at the α-location of the ether bond takes place, where the hydrogen atom located at the α-position in relation to

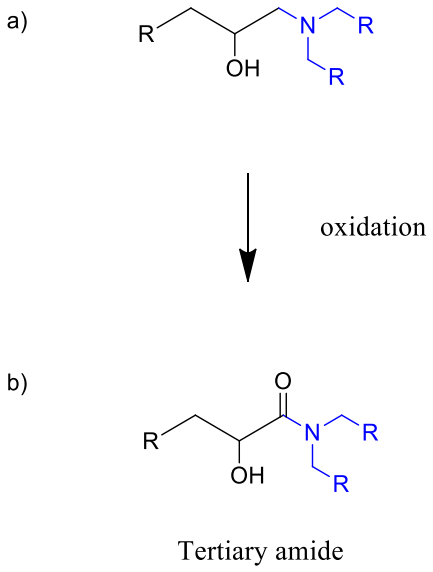

Fig. 6. (a) Generic structure of a fully cured epoxy-amine network; (b) formation of tertiary amides through oxidation reactions.

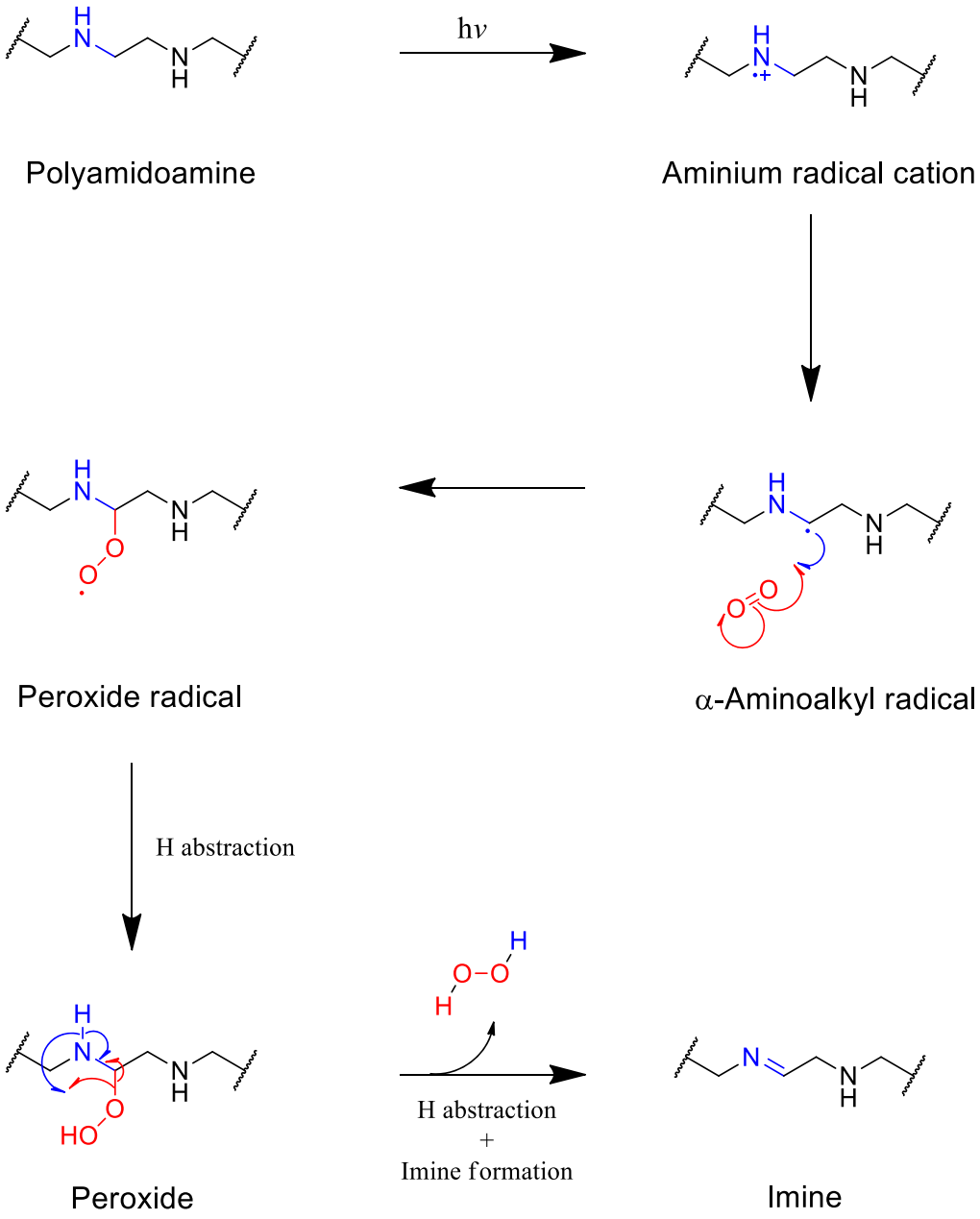

Fig. 7. Formation of imines.

the oxygen atoms of the ether group is primarily abstracted. Subsequently, hydroperoxides are formed from the abstraction of the readily available hydrogen atoms from the polymeric backbones. Further thermooxidative and photooxidative degradation of hydroperoxides would then result in the formation of an alkoxy radical, followed by the formation of phenyl formate end groups during hydrolysis and chain scission reactions.

On the other hand, the formation of new tertiary amides evident from the band at 1650 cm^{-1} would be through the abstraction of hydrogen from the α-methylene group, followed by the oxidation of amino methylenes in the network nodes as shown in Fig. 6 [4,7].

Apart from that, absorption band at 1650 cm^{-1} could also be attributed to the formation of imines, following the autooxidation mechanism of amines reported in Morsch, et al. [7] and the proposed mechanism is presented in Fig. 7.

Polyamidoamine is a common curing agent utilised in the formulation of anti-corrosive epoxy coatings based on Ramezanzadeh, et al. [62]. The photosensitivity of polyamidoamine has been extensively discussed in Arbeloa, et al. [63] where bathochromic shifts, triplet quenching and impact on electron movements were observed in dyes added with polyamidoamine as a result of various photochemical and photophysical interactions. It is proposed that polyamidoamine was present in the coating utilised in this research and that the oxidation process based on Fig. 7 has occurred.

Based on Fig. 7, the oxidation process begins with the removal of an electron from a secondary amine, leading to the creation of an aminium radical cation. The specific source of the initial one-electron oxidant is unclear, but it is suggested that it could be molecular oxygen or radicals originating from UV-absorbing aromatic groups in DGEBA. These UV-absorbing groups are known to initiate photo-ageing in similar phenoxy resins. Once these aminium radical cations are formed, they undergo rapid rearrangement to generate α-aminoalkyl radicals. Subsequently, these α-aminoalkyl radicals can then be transformed into radical iminium ions either directly through further one-electron oxidation or by forming peroxide species. The elimination of hydrogen peroxide then leads to the creation of unsaturated imine groups [7].

4. Conclusion

Epoxy amine coatings have demonstrated different surface and spectral responses towards hygrothermal ageing and artificial weathering that is comprised of UV accelerated degradation conditions and neutral salt spray test. A combination of ToF SIMS measurement and FTIR analysis has indicated the occurrence of hydrolysis, chain scission, crosslinking and oxidation reaction as a result of artificial weathering and hygrothermal ageing. PCA analysis of ToF-SIMS positive ion spectra illustrated that PC1 has collected information on a variation of surface responses caused by hydrolytic degradation, photooxidative and thermal oxidative degradation of epoxy amine coatings. On the other hand, PC2 has provided information on the photooxidative reaction on the surface of epoxy amine coatings where UV accelerated degradation conditions were involved. Artificial weathering conditions coupled with corrosion under insulation conditions have resulted in the most significant variation of FTIR spectra and the hydrolysis and photoxidation of epoxy amine coatings were also validated by FTIR analysis through the growth of two absorption bands at 1709 cm^{-1} and 1650 cm^{-1}, indicating the formation of carbonyl containing groups such as ketones, aldehydes, phenyl formates, imine or tertiary amides.

CRediT authorship contribution statement

Janice Xin Yee Ng: Writing – review & editing, Writing – original draft, Visualization, Validation, Methodology, Investigation, Formal analysis, Data curation, Conceptualization. **Nicholas Sheng Loong Tan:** Writing – review & editing, Validation, Investigation, Formal analysis, Data curation. **Wing Huen Chung:** Writing – review & editing, Validation, Formal analysis, Data curation. **Vladimir Golovanevskiy:** Writing – review & editing, Supervision. **Hanan Farhat:** Writing – review & editing, Supervision. **Thunyaluk Pojtanabuntoeng:** Writing – review & editing, Supervision.

Declaration of competing interest

The authors declare that they have no known competing financial interests or personal relationships that could have appeared to influence the work reported in this paper.

Data availability

Data will be made available on request.

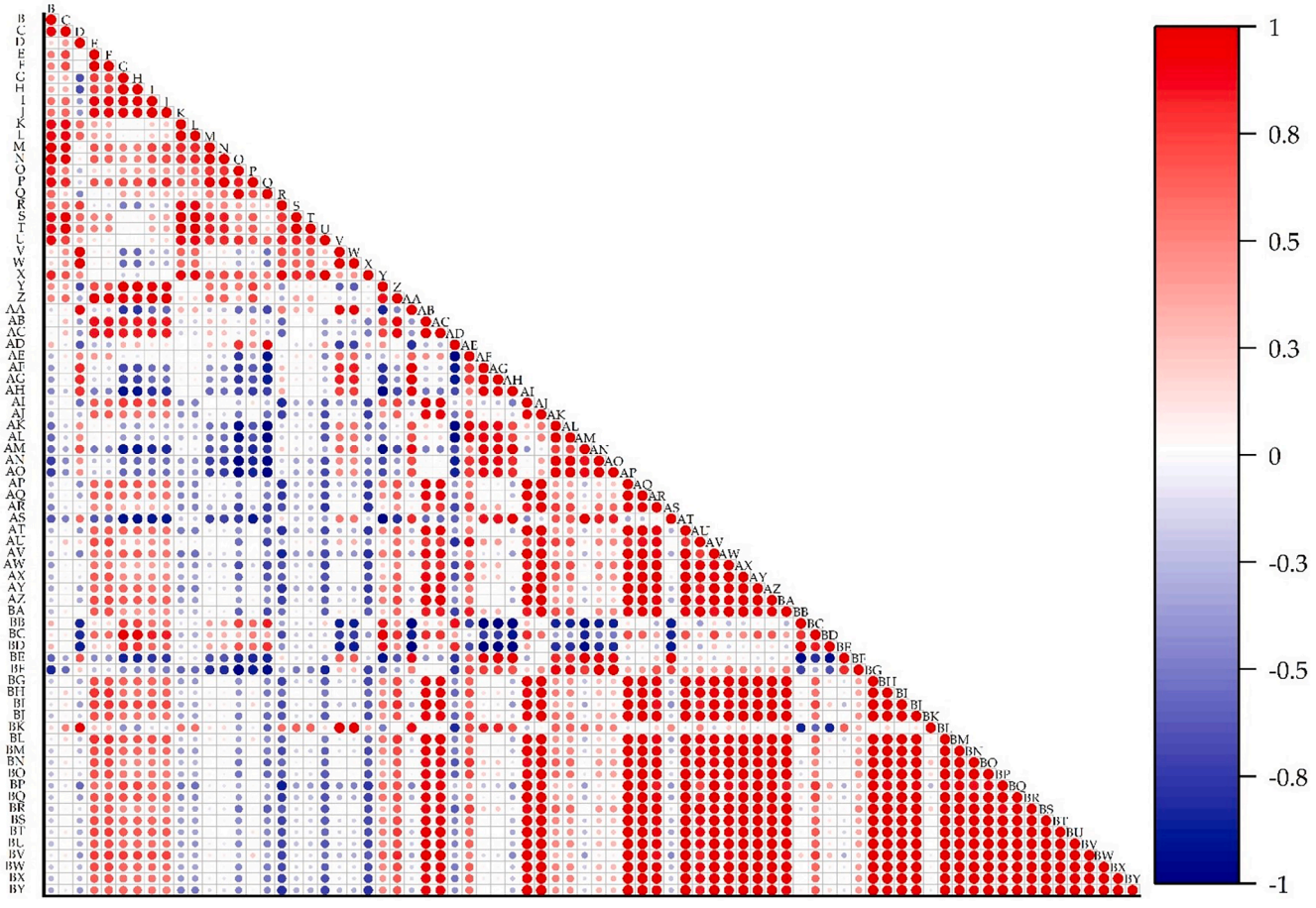

Correlation matrix of mass fragments included in principal component analysis.

Acknowledgement

This research is funded by Qatar Environment & Energy Research Institute (QEERI). IONTOF M6 ToF-SIMS at the John de Laeter Centre, Curtin University, was obtained using funding from the Australian Research Council LIEF program (LE190100053).

References

[1] A. Ghasemi-Kahrizsangi, J. Neshati, H. Shariatpanahi, E. Akbarinezhad, Improving the UV degradation resistance of epoxy coatings using modified carbon black nanoparticles, Prog. Org. Coat. 85 (2015) 199–207, https://doi.org/10.1016/j.porgcoat.2015.04.011, 2015/08/01/.
[2] Control of corrosion under thermal insulation and fireproofing materials—a systems approach, N. International, 2017 [Online]. Available: https://store.ampp.org/sp0198-2016.
[3] A. Palanisamy, N.V. Salim, J. Parameswaranpillai, and N. Hameed, "Water sorption and solvent sorption of epoxy/block copolymer and epoxy/thermoplastic blends," in Handbook of Epoxy Blends, J. Parameswaranpillai, N. Hameed, J. Pionteck, and E. M. Woo Eds. Cham: Springer International Publishing, 2016, ch. 37, pp. 1098–1110.
[4] C. Galant, B. Fayolle, M. Kuntz, J. Verdu, Thermal and radio-oxidation of epoxy coatings, Prog. Org. Coat. 69 (4) (2010) 322–329, https://doi.org/10.1016/j.porgcoat.2010.07.005, 2010/12/01/.
[5] P. Krishnan, Water sorption and solvent sorption behavior of epoxy/rubber polymer blends, in: J. Parameswaranpillai, N. Hameed, J. Pionteck, E.M. Woo (Eds.), Handbook of Epoxy Blends, Springer International Publishing, Cham, 2017, pp. 315–337.
[6] A. Shundo, S. Yamamoto, K. Tanaka, Network formation and physical properties of epoxy resins for future practical applications, JACS. Au 2 (7) (2022) 1522–1542, https://doi.org/10.1021/jacsau.2c00120, 2022/07/25.
[7] S. Morsch, et al., Examining the early stages of thermal oxidative degradation in epoxy-amine resins, Polym. Degrad. Stab. 176 (2020) 109147, https://doi.org/10.1016/j.polymdegradstab.2020.109147, 2020/06/01/.
[8] A.E. Krauklis, A.T. Echtermeyer, Mechanism of yellowing: carbonyl formation during hygrothermal ageing in a common amine epoxy, Polymers 10 (9) (2018) 1017 [Online]. Available: https://www.mdpi.com/2073-4360/10/9/1017.
[9] B. Mailhot, S. Morlat-Thérias, M. Ouahioune, J.L. Gardette, Study of the degradation of an epoxy/amine resin, 1, Macromol Chem Phys 206 (5) (2005) 575–584, https://doi.org/10.1002/macp.200400395, 2005/03/04.
[10] A. Rivaton, L. Moreau, J.L. Gardette, Photo-oxidation of phenoxy resins at long and short wavelengths—II. Mechanisms of formation of photoproducts, Polym. Degrad. Stab. 58 (3) (1997) 333–339, https://doi.org/10.1016/S0141-3910(97)00088-8, 1997/12/01/.
[11] S. Nikafshar, O. Zabihi, M. Ahmadi, A. Mirmohseni, M. Taseidifar, and M. Naebe, "The effects of UV light on the chemical and mechanical properties of a transparent epoxy-diamine system in the presence of an organic UV absorber," Materials, vol. 10, no. 2, 10.3390/ma10020180.
[12] Y. Malajati, S. Therias, J.L. Gardette, Influence of water on the photooxidation of KHJ® phenoxy resins, 1. Mechanisms, Polym. Degrad. Stab. 96 (1) (2011) 144–150, https://doi.org/10.1016/j.polymdegradstab.2010.10.007, 2011/01/01/.
[13] J. Delozanne, N. Desgardin, N. Cuvillier, E. Richaud, Thermal oxidation of aromatic epoxy-diamine networks, Polym. Degrad. Stab. 166 (2019) 174–187, https://doi.org/10.1016/j.polymdegradstab.2019.05.030, 2019/08/01/.
[14] F. Delor-Jestin, D. Drouin, P.Y. Cheval, J. Lacoste, Thermal and photochemical ageing of epoxy resin – Influence of curing agents, Polym. Degrad. Stab. 91 (6) (2006) 1247–1255, https://doi.org/10.1016/j.polymdegradstab.2005.09.009, 2006/06/01/.
[15] A. Rezig, et al., Relationship between chemical degradation and thickness loss of an amine-cured epoxy coating exposed to different UV environments, J. Coat Technol. Res. 3 (3) (2006) 173–184, https://doi.org/10.1007/BF02774507, 2006/07/01.
[16] D. Gibhardt, C. Buggisch, D. Meyer, B. Fiedler, Hygrothermal ageing history of amine-epoxy resins: effects on thermo-mechanical properties, in English, Front. Mater., Origin. Res. 9 (2022), https://doi.org/10.3389/fmats.2022.826076, 2022-March-02.
[17] A.E. Krauklis, A.I. Gagani, A.T. Echtermeyer, Hygrothermal ageing of amine epoxy: reversible static and fatigue properties, Open Eng. 8 (1) (2018) 447–454, https://doi.org/10.1515/eng-2018-0050.
[18] K. Xu, W. Chen, X. Zhu, L. Liu, Z. Zhao, G. Luo, Chemical, mechanical and morphological investigation on the hygrothermal ageing mechanism of a toughened epoxy, Polym Test 110 (2022) 107548, https://doi.org/10.1016/j.polymertesting.2022.107548, 2022/06/01/.
[19] A. Le Guen-Geffroy, P.Y. Le Gac, B. Habert, P. Davies, Physical ageing of epoxy in a wet environment: coupling between plasticization and physical ageing, Polym. Degrad. Stab. 168 (2019) 108947, https://doi.org/10.1016/j.polymdegradstab.2019.108947, 2019/10/01/.
[20] F. Awaja, P.J. Pigram, Surface molecular characterisation of different epoxy resin composites subjected to UV accelerated degradation using XPS and ToF-SIMS, Polym. Degrad. Stab. 94 (4) (2009) 651–658, https://doi.org/10.1016/j.polymdegradstab.2009.01.001, 2009/04/01/.
[21] B. Mailhot, S. Morlat-Thérias, P.O. Bussière, J.L. Gardette, Study of the degradation of an epoxy/amine resin, 2, Macromol Chem Phys 206 (5) (2005) 585–591, https://doi.org/10.1002/macp.200400394, 2005/03/04.
[22] G. Capiel, J. Uicich, D. Fasce, P.E. Montemartini, Diffusion and hydrolysis effects during water ageing on an epoxy-anhydride system, Polym. Degrad. Stab. 153 (2018) 165–171, https://doi.org/10.1016/j.polymdegradstab.2018.04.030, 2018/07/01/.
[23] M.A. Soto-Oviedo, M.A. De Paoli, Photo-oxidative degradation of poly (epichlorohydrin-co-ethylene oxide) elastomer at 254 nm, Polym. Degrad. Stab. 76 (2) (2002) 219–225, https://doi.org/10.1016/S0141-3910(02)00017-4, 2002/01/01/.
[24] S. Nikafshar, J. McCracken, K. Dunne, M. Nejad, Improving UV-Stability of epoxy coating using encapsulated halloysite nanotubes with organic UV-Stabilizers and lignin, Prog. Org. Coat. 151 (2021) 105843, https://doi.org/10.1016/j.porgcoat.2020.105843, 2021/02/01/.
[25] F. Awaja, M. Gilbert, B. Fox, G. Kelly, P.J. Pigram, Investigation of the postcure reaction and surface energy of epoxy resins using time-of-flight secondary ion mass spectrometry and contact-angle measurements, J. Appl. Polym. Sci. 113 (5) (2009) 2755–2764, https://doi.org/10.1002/app.301352009/09/05.
[26] D.J. Graham, D.G. Castner, Multivariate analysis of tof-sims data from multicomponent systems: the why, when, and how, Biointerphases 7 (1) (2012) 49, https://doi.org/10.1007/s13758-012-0049-3.
[27] S. Brand, L. Veith, R. Baier, C. Dietrich, M.J. Schmid, T.A. Ternes, New methodical approaches for the investigation of weathered epoxy resins used for corrosion protection of steel constructions, J. Hazard. Mater. 395 (2020) 122289, https://doi.org/10.1016/j.jhazmat.2020.122289, 2020/08/05/.
[28] N. Nikitas, D.I. Tzaras, I. Triandafillidi, C.G. Kokotos, Photochemical oxidation of benzylic primary and secondary alcohols utilizing air as the oxidant, Green Chemistry 22 (2020) 471–477, https://doi.org/10.1039/C9GC03000J.
[29] M.C. Biesinger, P.Y. Paepegaey, N.S. McIntyre, R.R. Harbottle, N.O. Petersen, Principal component analysis of TOF-SIMS images of organic monolayers, Anal. Chem. 74 (22) (2002) 5711–5716, https://doi.org/10.1021/ac020311n, 2002/11/01.
[30] A.A. Galuska, ToF-SIMS determination of molecular weights from polymeric surfaces and microscopic phases, Surface Interface Analy. 25 (10) (1997) 790–798,, https://doi.org/10.1002/(SICI)1096-9918(199709)25:10<790::AID-SIA301>3.0.CO;2-F.
[31] X.V. Eynde, P. Bertrand, ToF-SIMS quantification of polystyrene spectra based on principal component analysis (PCA)†, Surface Interface Analy. 25 (11) (1997) 878–888, 10.1002/(SICI)1096-9918(199710)25:11<878::AID-SIA311>3.0.CO;2-C.
[32] F. Awaja, G. van Riessen, G. Kelly, B. Fox, P.J. Pigram, ToF-SIMS investigation of epoxy resin curing reaction at different resin to hardener ratios, J. Appl. Polym. Sci. 110 (5) (2008) 2711–2717.
[33] ISO 12944-6:2018, Paints and varnishes — corrosion protection of steel structures by protective paint systems — part 6: laboratory performance test methods, The International Organisation for Standardization, 2018 [Online]. Available: https://www.iso.org/obp/ui/en/#iso:std:iso:12944:-6:ed-2:v1:en.
[34] Y. Yang, A.B. Bodington, B.T.A. Chang, Evaluation of protective coatings to mitigate corrosion under insulation, in: presented at the CORROSION 2016, 2016.
[35] ISO 19277:2018, Petroleum, petrochemical and natural gas industries — qualification testing and acceptance criteria for protective coating systems under insulation, The International Organisation for Standardization, Switzerland, 2018.
[36] M.W. Akhtar, J.S. Kim, M.A. Memon, M.Y. Khan, M.M. Baloch, Surface modification of magnesium oxide/epoxy composites with significantly improved mechanical and thermal properties, Mater. Electr. 32 (11) (2021) 15307–15316.
[37] A.A. Wereszczak, et al., Thermally conductive MgO-filled epoxy molding compounds, IEEE Transact. Compon., Package. Manufactur. Techn. 3 (12) (2013) 1994–2005, https://doi.org/10.1109/TCPMT.2013.2281212.
[38] D. Zhu, et al., Investigation of magnesium hydroxide functionalized by polydopamine/transition metal ions on flame retardancy of epoxy resin, J Therm Anal Calorim 147 (23) (2022) 13301–13312, https://doi.org/10.1007/s10973-022-11467-5.
[39] A. Jelić, et al., Determination of mechanical properties of epoxy composite materials reinforced with silicate nanofillers using digital image correlation (DIC), in eng, Polymers. 14 (6) (2022), https://doi.org/10.3390/polym14061255. Mar 21.
[40] T. Ohta, K. Iida, Effect of magnesium hydroxide on voltage lifetime of epoxy composites, Electr. Commun. Japan 99 (2) (2016) 10–18, https://doi.org/10.1002/ecj.11769, 2016/02/01.
[41] A. Viretto, et al., Thermal degradation of polyesters filled with magnesium dihydroxide and magnesium oxide, Fire Mater. 40 (3) (2016) 445–463, https://doi.org/10.1002/fam.2299, 2016/04/01.
[42] A. Rivaton, L. Moreau, J.L. Gardette, Photo-oxidation of phenoxy resins at long and short wavelengths—I. Identification of the photoproducts, Polym. Degrad. Stab. 58 (3) (1997) 321–332, https://doi.org/10.1016/S0141-3910(97)00089-X, 1997/12/01/.
[43] S. Nikafshar, O. Zabihi, M. Ahmadi, A. Mirmohseni, M. Taseidifar, M. Naebe, The effects of UV light on the chemical and mechanical properties of a transparent epoxy-diamine system in the presence of an organic UV absorber, in eng, Materials. 10 (2) (2017), https://doi.org/10.3390/ma10020180. Feb 14.
[44] D.A. Powers, Interaction of water with epoxy, Sandia National Laboratories (SNL), Albuquerque, NMLivermore, CA (United States), United States, 2009. SAND2009-4405, 2009-07-01.

[45] C.L. Soles, A.F. Yee, A discussion of the molecular mechanisms of moisture transport in epoxy resins, Polymer Phys. 38 (5) (2000) 792–802. 10.1002/(SICI)1099-0488(20000301)38:5<792::AID-POLB16>3.0.CO;2-H.
[46] S.S. Sambaza, A. Maity, K. Pillay, Polyaniline-coated tio2 nanorods for photocatalytic degradation of bisphenol a in water, ACS. Omega 5 (46) (2020) 29642–29656, https://doi.org/10.1021/acsomega.0c00628, 2020/11/24.
[47] P. Chen, et al., The Role of Methyl Groups in the Early Stage of Thermal Polymerization of Polycyclic Aromatic Hydrocarbons Revealed by Molecular Imageing, Energy Fuels 35 (3) (2021) 2224–2233, https://doi.org/10.1021/acs.energyfuels.0c04016, 2021/02/04.
[48] F. Awaja, G. van Riessen, B. Fox, G. Kelly, P.J. Pigram, Time-of-flight secondary ion mass spectrometry investigation of epoxy resin curing behavior in real time, J Appl Polym Sci 113 (5) (2009) 2765–2776, https://doi.org/10.1002/app.30136.
[49] L. Zheng, et al., Fabrication of a nano-biocatalyst for regioselective acylation of arbutin, Green. Chem. Lett. Rev. 11 (2) (2018) 55–61, https://doi.org/10.1080/17518253.2018.1437226, 2018/04/03.
[50] Y. Yu, X. Fei, J. Tian, L. Xu, X. Wang, Y. Wang, Self-assembled enzyme–inorganic hybrid nanoflowers and their application to enzyme purification, Biointerfaces 130 (2015) 299–304, https://doi.org/10.1016/j.colsurfb.2015.04.033, 2015/06/01/.
[51] S.T. Knox, A. Wright, C. Cameron, J.P.A. Fairclough, Structural variation and chemical performance—a study of the effects of chemical structure upon epoxy network chemical performance, ACS. Appl. Polym. Mater. 3 (7) (2021) 3438–3445, https://doi.org/10.1021/acsapm.1c00378, 2021/07/09.
[52] M.A. Escola, C.A. Moina, A.C. Niño Gómez, G.O. Ybarra, The determination of the degree of cure in epoxy paints by infrared spectroscopy, Polym Test 24 (5) (2005) 572–575, https://doi.org/10.1016/j.polymertesting.2005.02.013, 2005/08/01/.
[53] Y. Hao, F. Liu, E.H. Han, S. Anjum, G. Xu, The mechanism of inhibition by zinc phosphate in an epoxy coating, Corros Sci 69 (2013) 77–86, https://doi.org/10.1016/j.corsci.2012.11.025, 2013/04/01/.
[54] A. Rivaton, Recent advances in bisphenol-A polycarbonate photodegradation, Polym. Degrad. Stab. 49 (1) (1995) 163–179, https://doi.org/10.1016/0141-3910(95)00069-X, 1995/01/01/.
[55] S. Le Craz, R.A. Pethrick, Solvent effects on cure 1-benzyl alcohol on epoxy cure, Internat. J. Polym. Mater. Polym. Biomater. 60 (7) (2011) 441–455, https://doi.org/10.1080/00914037.2010.531813, 2011/06/15.
[56] Y.R. Luo, Comprehensive handbook of chemical bond energies, CRC Press, 2007.
[57] N.D. Searle, Environmental Effects on Polymeric Materials, Plast. Environ. (2003) 311–358.
[58] R.N. Clark, J.M. Curchin, T.M. Hoefen, G.A. Swayze, Reflectance spectroscopy of organic compounds: 1. Alkanes, Planets 114 (E3) (2009), https://doi.org/10.1029/2008JE003150, 2009/03/01.
[59] F.S. Parker, Amides and amines, in: F.S. Parker (Ed.), Applications of infrared spectroscopy in biochemistry, biology, and medicine, Springer US, Boston, MA, 1971, pp. 165–172.
[60] R. Mahmudzade, P. Nikaeen, W. Chirdon, A. Khattab, D. Depan, Photodegradation mechanisms and physico-chemical properties of EPON-IPD epoxy-based polymers, React. Funct. Polymers 178 (2022) 105351, https://doi.org/10.1016/j.reactfunctpolym.2022.105351, 2022/09/01/.
[61] E. Yousif, R. Haddad, Photodegradation and photostabilization of polymers, especially polystyrene: review, Springerplus 2 (2013) 398, https://doi.org/10.1186/2193-1801-2-398.
[62] M. Ramezanzadeh, B. Ramezanzadeh, M.G. Sari, M.R. Saeb, Corrosion resistance of epoxy coating on mild steel through polyamidoamine dendrimer-covalently functionalized graphene oxide nanosheets, J. Industr. Eng. Chem. 82 (2020) 290–302, https://doi.org/10.1016/j.jiec.2019.10.025, 2020/02/25/.
[63] E.M. Arbeloa, C.M. Previtali, S.G. Bertolotti, A comparative study on the photophysics and photochemistry of xanthene dyes in the presence of polyamidoamine (PAMAM) dendrimers, Chemphyschem. 19 (8) (2018) 934–942, https://doi.org/10.1002/cphc.201701295.